5-2004

Viscogenic Effects on the Relaxation Kinetics of Bovine Serum Albumin: Preliminary Experiments for Investigating Altered Fluid Dynamics in Microgravity

Jason Corey Bell

Viscogenic Effects on the Relaxation Kinetics of Bovine Serum Albumin: Preliminary Experiments for Investigating Altered Fluid Dynamics in Microgravity

An Undergraduate Thesis by

Jason C. Bell

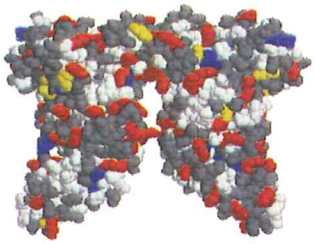

Louisiana State University
May 2004

Table of Contents

Abstract

In order to determine whether altered fluid dynamics in microgravity are the direct cause of the physiological effects experienced by humans during space flight, we have begun characterizing the binding kinetics of several protein-ligand systems. One of these proteins, Bovine Serum Albumin (BSA), is thought to bind its substrates in a diffusion-controlled manner. In order to determine whether a protein is actually diffusion-limited rather than simply very fast, the kinetics of interest must be characterized as a function of viscosity. The relaxation kinetics of the interaction of BSA and a fluorescent probe, 1-anilino-8-napththalenesulfonate (ANS) were characterized at five different viscosities (% glycerol) using a stopped-flow rapid mixing apparatus. The data were then fit to several models to determine the relationship between viscosity and the kinetic rate constants. While the data we have collected does not conclusively prove that the association of BSA and ANS is diffusion-limited, the kinetics are dramatically slowed by increasing viscosity, a hallmark of diffusion-limited reactions. Our lab's intent is to characterize the kinetics of several proteins, and thus several different 'types' of kinetic interactions, on NASA's KC-135 airplane during parabolic flights that simulate microgravity.

Introduction

Since the 1960's when NASA began its human space flight program, scientists and physicians have observed various physiological side effects as a result of microgravity. These phenomena can vary from serious medical risks such as bone resorption or muscle atrophy to seemingly trivial side effects such as nausea, headaches, disorientation, insomnia etc. For just as long as physicians have been aware of these physiological stresses, scientists have also known that fluid dynamics are also altered in the absence of gravity. For instance, a drop of virtually any liquid becomes perfectly spherical in microgravity, where forces such as surface tension and intermolecular interactions prevail. While these changes in fluid dynamics have presented technical problems for engineers for decades, biologists have recently taken advantage of them. Specifically, protein crystallographers have found that they can grow significantly larger crystals in microgravity, allowing for the three dimensional mapping of structures for proteins that were previously unattainable in the presence of gravity[1].

Given the lack of scientific evidence implicating any particular cell or bio-molecule in the aforementioned physiological phenomena, our lab proposes that the altered fluid dynamics in microgravity is the primary cause of changes in biochemical interactions, resulting in physiological effects. Specifically, we postulate that the characteristics of diffusion in the absence of gravity are different than on Earth. Given that many proteins and enzymes have evolved to become limited only by the rate of diffusion, it is possible that the physiological side effects experienced by humans in microgravity could be attributed the altered kinetics of these proteins.

While it is tempting to hypothesize that diffusion will slow down, it is possible that the lack of gravity may allow some intermolecular forces to dominate in a reaction where they were previously opposed by gravity and/or diffusion. In order to test this hypothesis, the diffusion-limited association of Bovine Serum Albumin with 8-Anilino-1-naphthalenesulfonate has been characterized using a stopped-flow rapid mixing apparatus coupled to a fluorometer. This reaction and several others will be experimentally analyzed on NASA's KC-135 airplane during parabolic flights that simulate microgravity (see Figure 1).

The interaction of biological macromolecules with small molecules and each other is both dynamically complex and beautifully simple. While very complex mechanisms and equations like the Monod-Wyman-Changeux (MWC) and Koshland-Némethy-Filmer (KNF) models for cooperative binding have been formulated to describe these processes, these biochemical interactions are the molecular foundation of living organisms[2]. The study of biophysical chemistry and thermodynamics focuses on how subtle changes in parameters such as pH, salt concentration and temperature are critical to the proper functioning of a protein. The primary focus of this thesis is how the rate of protein-ligand interactions are affected by diffusion and how these rates could be implicated in the physiological side effects observed in organisms in microgravity.

For any association reaction to occur, the molecules involved must collide with each other, or at least come close enough for their electrostatic fields to interact. In the event of protein-ligand binding or enzyme catalysis, many of these collisions have a null effect because the active site of the protein involved fails to interact with the ligand, possibly because of incorrect orientation,

Protein

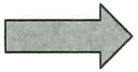

Protein with ligand bound

Each protein in the body binds to its own unique ligand. "Ligand" is a general name for a small molecule that binds to a protein.

Some of these interactions are very fast.

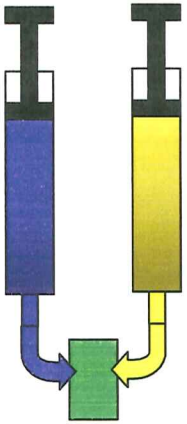

In the lab, the protein and its ligand are rapidly mixed to determine how fast they associate.

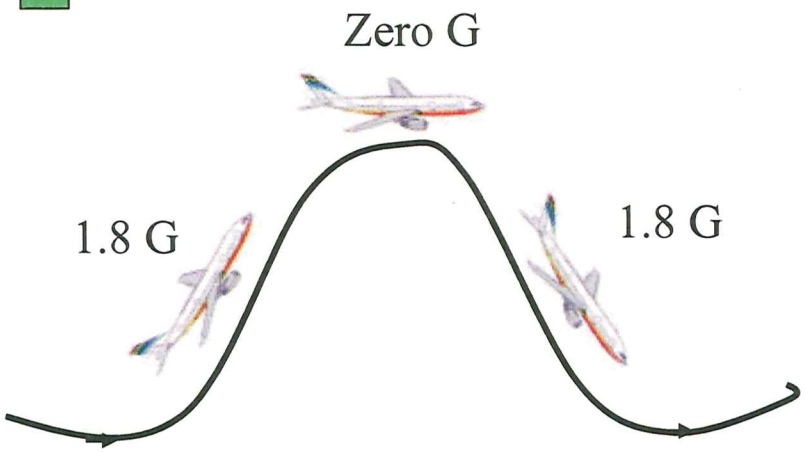

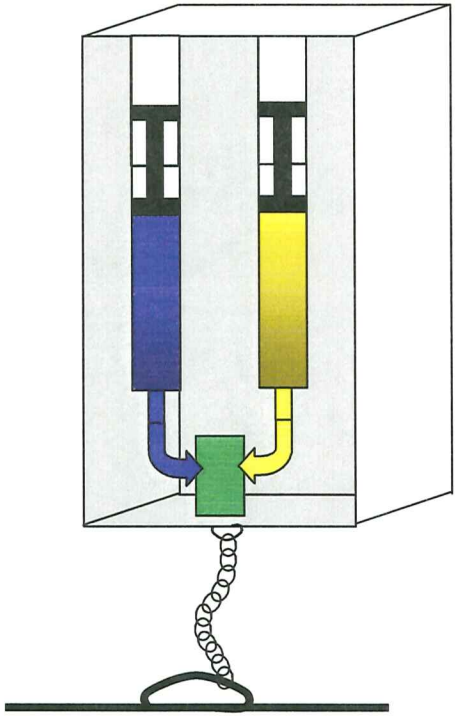

(floor of the plane)

On NASA's KC-135 airplane, protein and ligand will be rapidly mixed to determine how the absence of gravity affects the speed of the protein-ligand interaction.

Figure 1: Overview of the experimental design to determine the effect of microgravity on fluid dynamics and consequently protein-ligand interactions

occupation of the binding site with another molecule or some form of steric hindrance (just to list a few examples). The net rate of binding or catalysis is further impeded by the specific protein's rate-limiting step, whether it be a conformational change, the formation of a transition-state complex, etc. The slowest molecular process in the kinetic event is known as the rate-limiting step, which effectively follows a "bottle-neck principle" in which the fastest parts of a reaction cannot exceed its slowest counterpart. Evolution has dictated that some biological processes become so efficient that they are limited only by the rate at which diffusion can carry them into interaction with their ligand. Such proteins and enzymes are said to be diffusion-limited. Proteins that have been shown to be diffusion-limited via viscogenic studies include acetylcholinesterase[3], adenosine deaminase[4], β-lactamase I[5], carbonic anhydrase[6], chymotrypsin[7], hemoglobin[8], insulin[9], replication protein A[10], protein kinase C[11], and triosphosphate isomerase[13]. Non-specific protein phosphorylation in signal transduction has also been shown to be diffusion-limited; however, not through viscogenic studies[12]. Other unique processes that are diffusion-limited include the interaction of unfolded peptides with *Escherichia coli* Chaperone SecB[13], the folding of the α subunit of tryptophan synthase[14], the lateral lipid distribution in cell membranes (diffusion in two dimensions)[15] and the enzymatic catalysis of ribonuclease A along a strand of RNA (diffusion in one dimension)[16].

While the molecular interaction of bio-molecules is dynamic and complicated, the phenomenon of diffusion is intrinsically and mathematically staggering in its complexity, especially when applied to biological systems. Diffusion as a *descriptive* term is relatively straight forward, often taken to mean the spreading of a substance from a local origin. Such an event can be visualized by dropping ink into a glass of water and sensed by smell when someone wearing perfume walks

into a room. The *scientific* term for diffusion is much more limiting, taken from the OED: "diffusion: *Physics* The permeation of a gas or liquid between the molecules of another fluid placed in contact with it; the spontaneous molecular mixing or interpenetration of two fluids without chemical combination."

The *mathematical* definition of diffusion was taken to an even higher level when in 1906 Marian von Smoluchowski and Albert Einstein both independently explained Fick's First Law of Diffusion in molecular terms with the phenomenon of Brownian motion. (Refer to pg 17 for the derivation and further explanation of the Einstein-Smoluchowski equation). While this theory has been developed into many more complex models, the classical model is more than sufficient for the purposes of this thesis. In short, these models predict that the kinetic rate of diffusion-limited association should be in the range of 10^7 to 10^{11} $M^{-1}s^{-1}$. Furthermore, the model predicts an inverse dependence on the viscosity of the solution; allowing for a relatively simple and conclusive test for diffusion-limited biochemical reactions[18].

Bovine Serum Albumin and 8-Anilino-1-naphthalenesulfonate

The kinetic association of BSA and ANS was first characterized using a stopped-flow apparatus by Hiromi et al in 1976; however, they noticed a fast kinetic reaction that was could not be resolved by their instrument[19]. In 1987, Regenfuss and Clegg developed a fast-flow microsecond mixer for their stopped-flow apparatus and found the association of BSA-ANS to be $5E^8$ $M^{-1}s^{-1}$ at 22° C when mixed in 1:1 stoichiometric ratios[20]. Based on this kinetic rate and the theoretical rates as defined by the Einstein-Smoluchowski equation, they assumed that the reaction was diffusion-limited. No evidence confirming this assumption via viscosity dependent kinetic characterization has yet been published.

Bovine Serum Albumin is a lipid transport protein in the serum of cows. It is a well studied and widely used protein for various common laboratory experiments (e.g. the Bradford Assay) and is often added to protein stocks to stabilize the protein of interest and prevent its degradation[21]. The human analog (HSA shown in Figures 2 and 4) is involved in drug delivery as well as lipid transport, for example it is known to bind and transport Warfarin with diffusion-limited *and* allosteric kinetics[22]. Wafarin (a.k.a. Coumadin) is an anticoagulant that inhibits the synthesis of clotting factors; it is primarily used as both a therapy for heart patients with blood clots and as rat poison. The opportunity to confirm the diffusion-limited kinetics of BSA as well as its cost-effectiveness, storage stability and easy quantification contributed to the decision to use BSA for these experiments.

8-Anilino-1-naphthalenesulfonate (ANS, Figure 3) is a fluorescent probe commonly used to study lipid binding proteins. The wavelength scans of BSA, ANS and BSA·ANS shown in

Figure 5 demonstrates the change in fluorescence of ANS upon binding. The intrinsic fluorescence of ANS is quenched by water; however, when bound to hydrophobic regions of proteins the fluorescent emission at 470 nm dramatically increases when excited at 369 nm. The proximity of ANS to tryptophan in BSA can also be observed at 470 nm via resonant energy transfer by exciting the complex at 280 nm[23], where ANS absorbs the fluorescent emission of tryptophan at 350 nm resulting in secondary emission at 470 nm. ANS is also known to bind to cationic residues and hydrophobic patches on proteins- Figure 3 shows all the possible binding sites for ANS on HSA (for the purpose of demonstration we will assume that these sites are roughly equivalent to the ~ 100 binding sites on BSA)[24].

Human Serum Albumin

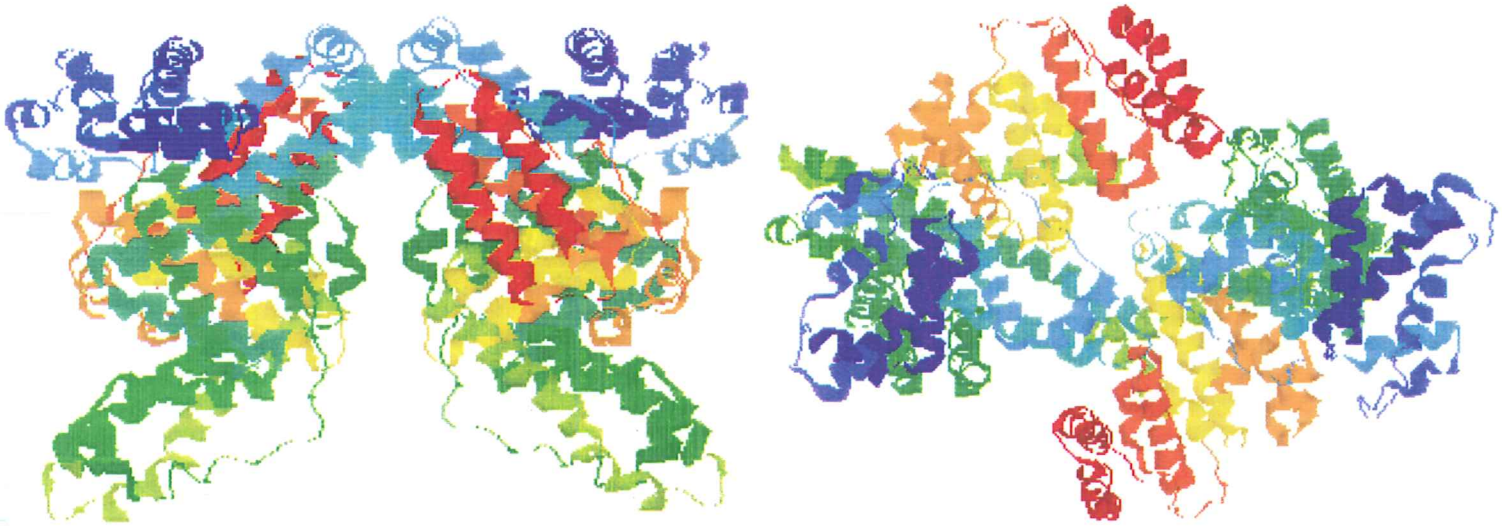

side view top view

Figure 2: Crystal structure of Human Serum Albumin (PDB 1AO6)[6]. HSA is believed to be a structural and functional analog of Bovine Serum Albumin (no crystal structure available), which was the primary protein studied.

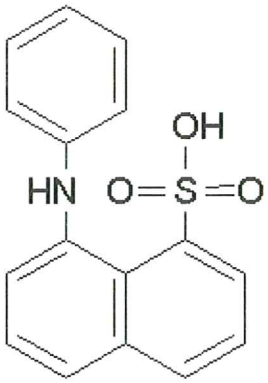

Figure 3:
8-Anilino-1-naphthalenesulfonate (ANS). ANS fluoresces at 470 nm when excited at 369.

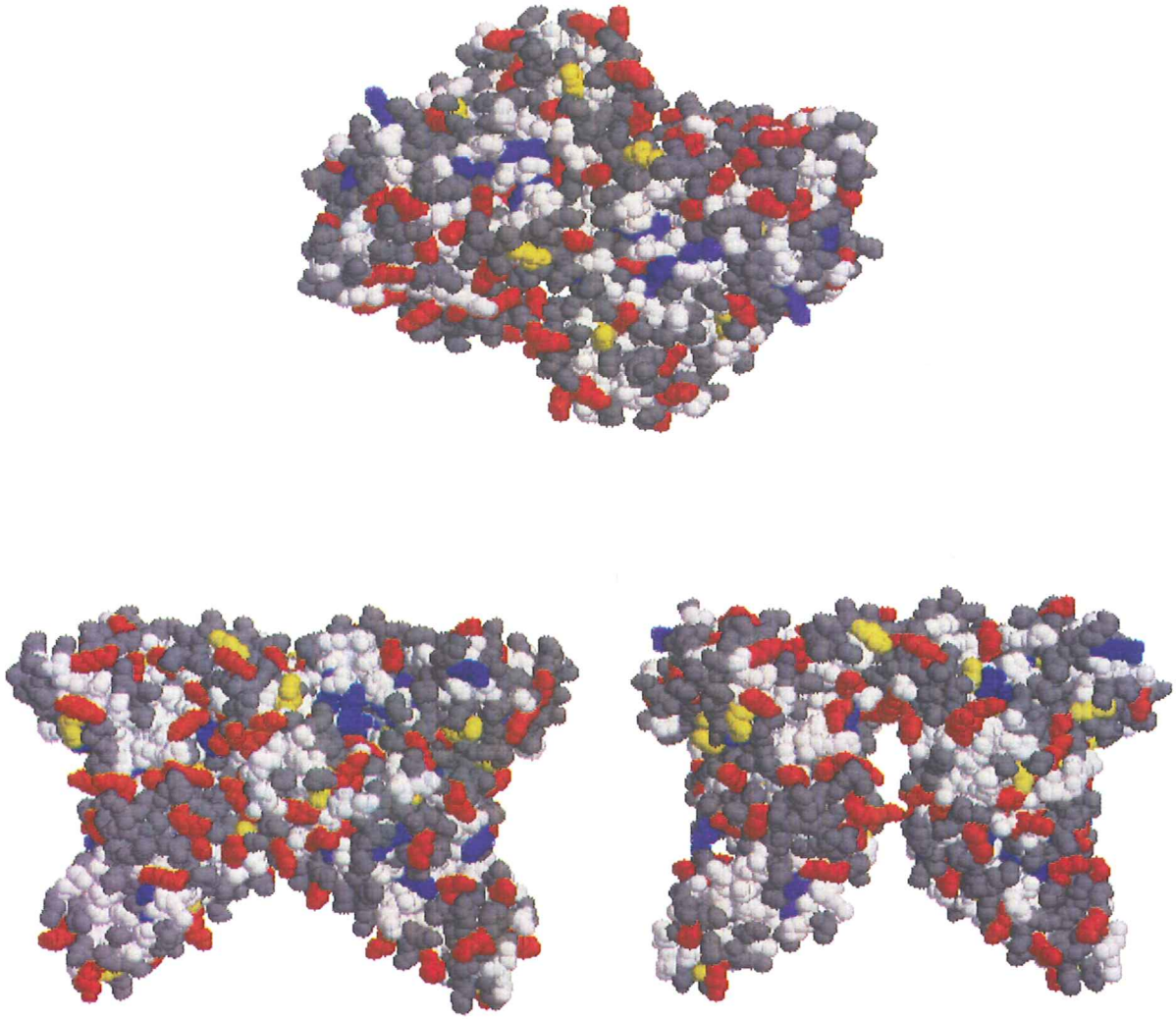

Figure 4: Three views of the crystal structure of Human Serum Albumin (PDB 1AO6)[6]. Residues are color coded to indicate possible binding sites for ANS, a negatively charged fatty acid. Color coding is as follows:

Tryptophan = green* (buried)
Arginine = blue
Lysine = red
Histidine = yellow
Hydrophobic = white
All others = gray

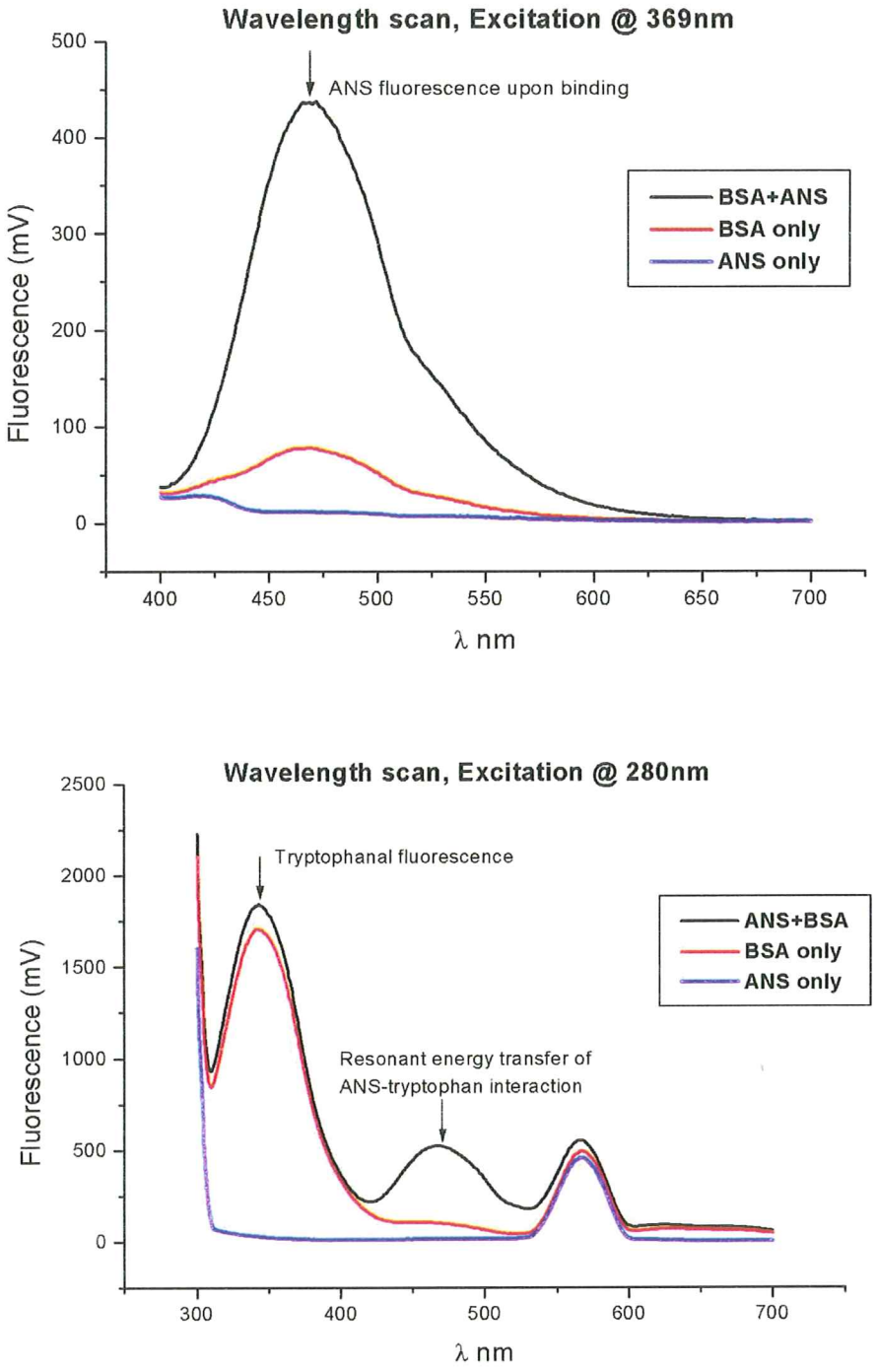

Figure 5 A) The top panel shows the emission spectra of ANS (blue), BSA (red) and the ANS-BSA complex (black) upon excitation at 369 nm. When bound to the hydrophobic pockets of BSA, the fluorescence increases 4 to 5x. **B)** The bottom panel demonstrates the resonant energy transfer between the aromatic amino acids of BSA, primarily tryptophan, and ANS. Lines are the same as in panel A, only excitation is at 280 nm in panel B.

Stopped-Flow Rapid Mixing

While the conceptual design for a stopped-flow apparatus is quite simple, it should by duly noted that stopped-flows are extremely delicate instruments of which much time and patience must be invested. On the most basic level, a stopped-flow is comprised of three or more mechanical syringes driven by extremely sensitive motors. These syringes are coupled appropriately to allow for variable mixing of two solutions (i.e. in order to vary concentration). The mixed solutions are pushed into cuvette which has an apparatus called a hard stop attached to it to compensate for pressure changes and rapidly stop the flow of the solutions through the cuvette. The instrument is coupled to a detection device, usually a spectrophotometer or a fluorometer and is configured to collect data within ~ 3 milliseconds after the solution is completely mixed[29].

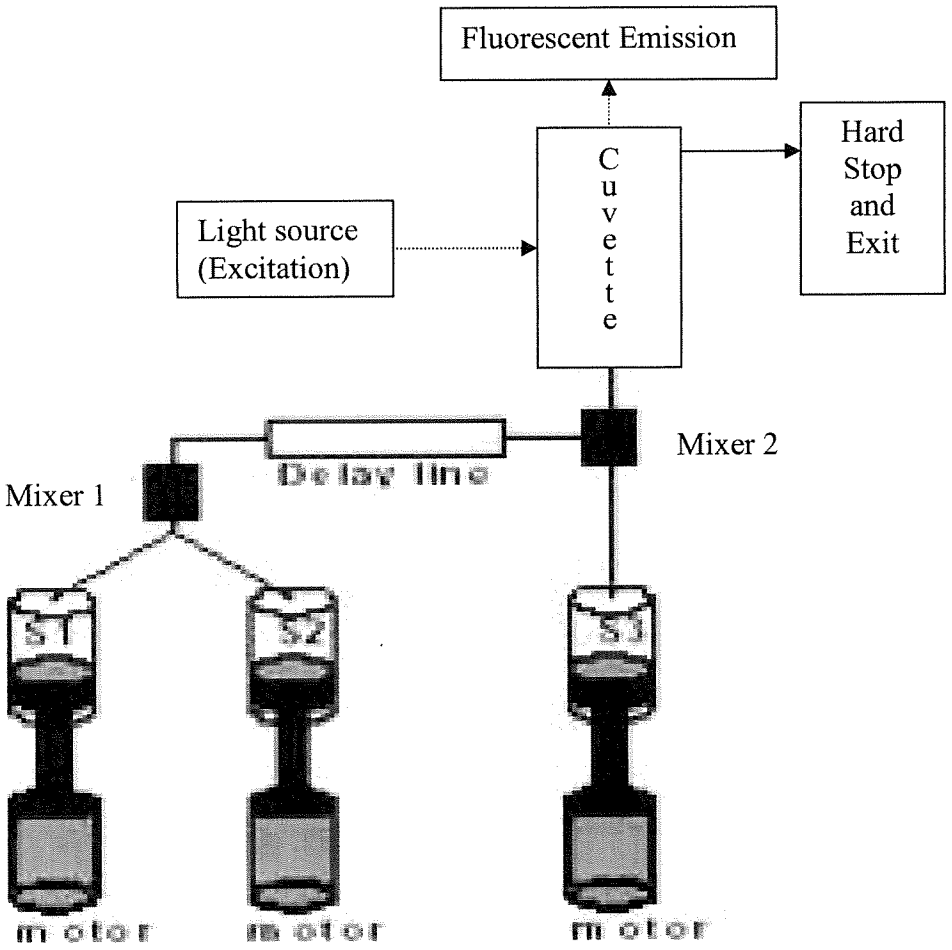

Figure 6: A schematic diagram of the basic design of a stopped flow apparatus. Syringes 1 and 2 are filled with buffer and protein while syringe 3 is filled with ligand. This allows for variable mixing ratios for S1 and S2, resulting in changes in [protein] while [ligand] remains constant throughout the experiment. When coupled to a fluorometer, light enters the cuvette 90° relative to the PMT. The total time required for mixing and flowing through the delay line (i.e. the dead time) is ~ 3-4 ms.

Methods and Approaches to Data Analysis

Relaxation kinetics is the study of a chemical system that has been perturbed by a jump in concentration, temperature, pressure, etc. The data collected is described by an exponential decay in which the components of the system "relax" back to equilibrium. Specifically, we used the concentration jump method, in which the [ANS] was held constant, while the [BSA] was varied by first mixing with buffer, then with the substrate. The rapid mixing of protein and ligand resulted in an approximate dead time of 3.0 milliseconds, the entire reaction was observed over a 300 ms time interval. In short, one can watch the reaction in "real time". This approach is very different from standard Michaelis-Menton kinetics that are performed at "steady-state".

The data collected is fit to the single exponential equation:

Equation 1: $$Y = (F_{max} - F_o) \bullet e^{(-(T - Toffset)/\tau) + Fo}$$

Where:
F_{max} = maximum fluorescence
F_o = initial fluorescence
T = time
T_{offset} = dead time + mixing time of the instrument
τ (tau) = time constant of association in seconds = $1/k_{obs}$

Figure 6 shows a simulated single exponential curve generated by Equation 1. A simple estimation of k_{obs} can be obtained by determining the time at which 63% of the reaction is over. Such an estimation is possible because at time = tau, the relationship simplifies to $1 - 1/e \approx .63$.

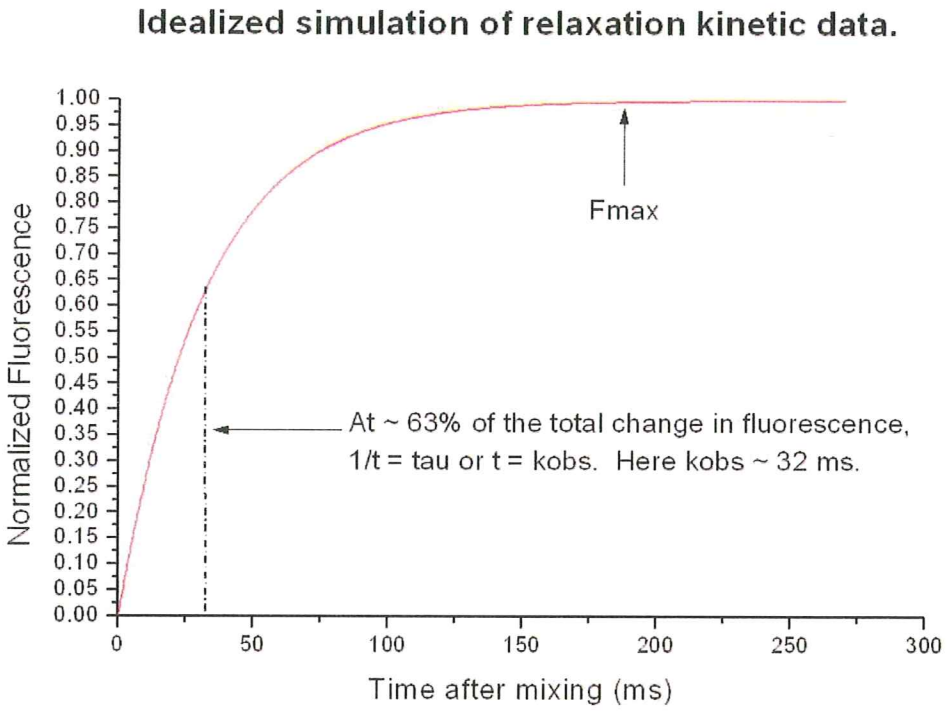

Figure 7: Simulated data for relaxation kinetics. Experimental data must be adjusted along the x axis via the T_{offset} term and along the y axis via the F_o term.

Obtaining k_{on} and k_{off}

In order to obtain k_{on} and k_{off} for a simple A + B ↔ C reaction, the inverse of the time constant τ is then plotted versus the sum of the equilibrium concentrations of protein and ligand to form a linear relationship. $1/\tau$ is known as k or k_{obs} (s^{-1}). For a simple bimolecular process (A + B↔C) the following relationship holds:

$$\mathbf{k_{obs} = k_{on} ([E] + [S]) + k_{off}}$$

Where:
k_{on} = the rate of association
k_{off} = the rate of disassociation
K_{obs} = fitted value from data at each concentration of reactants

In order to determine equilibrium concentrations, calculated concentrations are first plotted versus k_{obs}. This plot gives preliminary values for k_{on}, k_{off}, and allows one to calculate a Kd, where $Kd = k_{off}/k_{on}$. The inverse of this preliminary Kd and the quadratic equation are used to determine equilibrium concentrations of protein and ligand, which are again plotted versus kobs. This process is iteratively repeated twenty times in order to insure excellent convergence[26]. This procedure was followed for a previous study of the kinetics of ALBP + ANS[41]; however, anomalies in the data for BSA made this process impractical. The presence of these anomalies is presumably due to the more complex interaction of BSA with ANS. For a detailed review of relaxation theory, refer to Claude Bernasconi's *Relaxation Kinetics*[26].

Stretched Exponential Fitting of Raw Kinetic Data

In addition to the A + B ↔ C relaxation model above, data were fit to a more complex relaxation equation as defined by the Kohlrausch-Williams-Watts (KWW) stretched exponential function[37]. The KWW model is primarily used in the analysis of relaxation data obtained for the viscoelastic relaxation of glass; however, it has recently been applied to the analysis of complex biological systems involving Fluorescent Lifetime IMaging (FLIM) in heterogeneous biological tissues and anomalous diffusion of water in biological tissues[27].

The data collected were fit to the single exponential equation containing an additional exponential parameter β is added, which is restricted to be $0 < \beta < 1$ [26].

Equation 2: $$Y = (F_{max} - F_o) \bullet e^{((T - Toffset)/\tau)^{\beta}} + Fo$$

Under ideal experimental conditions, β would be a floating variable; however, when allowed to float for the data collected, false minima in the chi squared values and seemingly endless 'drift' in the iterative process resulted in poor non-linear fitting of the data; however, an approximate value of β =.6 was obtained in a majority of the fits, therefore β was set as a constant in order to determine reasonable k_{obs} values.. In addition to this stretched exponential, the sum of the concentrations was multiplied by the specific ratio of [BSA]/[ANS] in order to adjust for stoichiometric changes for each concentration jump[26]. The adjusted relationship is:

$$k_{obs} = k_{on} \mathbf{([BSA]/[ANS])*}([P] + [S]) + k_{off}$$

Fick's Law, Diffusion Limited Reactions and the Einstein-Smoluchowski Equation

When a chemical or biochemical rate for the association of two molecules is governed only by the frequency of their collision, the reaction is said to be diffusion controlled or diffusion limited. The frequency of these collisions is an upper limit that can be described using Fick's law of diffusion. There are several mathematical models that describe this process, the first of which was derived by Marian von Smoluchowski in 1917. The model assumes that two spheres of uniform size are driven towards each other by a concentration gradient[17].

Fick's first law of diffusion states that the flux is directly proportional to the distance gradient of the concentration, where flux is the quantity of some solute, or in this case a ligand (L), as it crosses a plane of area A in time.

Eq. 3 $$\text{Flux} = J = \frac{1}{A} \cdot \frac{dn_L}{dt} = D \cdot \frac{dc}{dx}$$

Where: J = Flux
A = area (m^2)
n_L = # of molecules of L
t = time (seconds)
c = concentration (M)
x = distance (m)
D = diffusion coefficient (m^2/s)

If we assume that a bulk of L is in a spherical distribution around a single molecule of P, then we get a surface area of interaction between P and L at a distance r. The flux becomes negative because the flow is in a direction so as to offset the gradient.

Eq. 4 $$J = -D_{PL} \cdot (4\pi r^2) \cdot \frac{d[L]}{dr}$$

Where: $D_{PL} = D_P + D_L$

Integration gives:

Eq. 5 $$J\, r_{PL}\int_{\infty} dr = -4\pi D_{PL}\, {}_0\int^{[L]o} d[L]$$

or

Eq. 6 $$\frac{J}{r_{PL}} = -4\pi D_{PL}[L]^o$$

The rate in this limit is:

Eq. 7 $$\frac{-d[P]}{dt} = k_{dc}[P][L]^o$$

Where: k_{dc} = the diffusion controlled rate constant; equivalent to k_{on}

Which is equal to the flux of L towards P:

Eq. 8 $$-J[P] = \frac{-d[L]}{dt}$$

When we combine and rearrange equations 5 and 6, we get:

Eq. 9 $$k_{dc} = \frac{-(d[P]/dt)}{[P][L]^o} = \frac{-J[P]}{[P][L]^o} = 4\pi D_{PL} r_{PL}$$

So, if we assume that $r_A \sim 40$ Å and $r_B \sim 3$ Å (values estimated from the crystal structures of HSA and ANS), we can calculate the diffusion coefficient D_{PL} using the Einstein-Stokes relationship and finally k_{dc}.

Eq. 10 $$D = \frac{k_B T}{6\pi r \eta}$$

Where: k_B = Boltzmann constant, $1.3807_E{}^{-23}$ ($kg \cdot m^2/K \cdot s^2$)
T = temperature in °K
r = radius of the molecule (m)
η = viscosity in Pascal seconds (kg/m·s)

If we assume the viscosity of our buffer is approximately the same as pure water at 6° C, then we can use the value of $1.6\ E^{-3}$ Pa•s.

So to calculate the theoretical rate for the interaction of ANS and BSA, assuming a net movement of ANS towards BSA…

$r_{PL} = 4_E^{-9}$ (m) + 3_E^{-10} (m) = **4.3_E^{-9} (m)**

$$D_{PL} = \frac{1.3807_E^{-23}\ (kg{\cdot}m^2/K{\cdot}s^2)(279°K)}{6\pi \cdot 4_E^{-9}\ (m) \cdot 1.6\ E^{-3}\ (kg/m{\cdot}s)} + \frac{1.3807_E^{-23}\ (kg{\cdot}m^2/K{\cdot}s^2)(279°K)}{6\pi \cdot 3_E^{-10}\ (m) \cdot 1.6\ E^{-3}\ (kg/m{\cdot}s)} = \mathbf{9.4}_E^{-11}\ \mathbf{(m^2/s)}$$

Finally…

$k_{dc} = 4\pi D_{PL} r_{PL} = 4_E^3\ (L/m^{-3}) \cdot \pi \cdot 6.02_E^{23}$ (molecules/mol) · 4.3_E^{-9} (m) · **9.4_E^{-11}** (m^2/s)

k_{dc} = 3.06 E^9 ($M^{-1}s^{-1}$) at 6° C

Considering that the radii used in the calculation assumed that both the protein and ligand are spheres, when in fact the structure of BSA is unknown and ANS is planar, the calculated value agrees satisfactorily with the experimental k_{on} determined from the standard model in no glycerol (see results). It should be noted that calculated values for k_{on} are almost *always* faster than experimentally determined values, usually by one or two orders of magnitude [29, 30, 31, 32].

Literature Review of the Effects of Microgravity: Correlations to Diffusion-Limited Proteins/Enzymes

While most of the scientific work on microgravity effects on biological systems has been conducted on a physiological or cellular level, I have attempted to correlate these known effects with diffusion limited processes. Because both the activity and the expression of tyrosine hydroxylase are decreased in microgravity[33], it serves as an excellent model for our hypothesis. Tyrosine hydroxylase (TH) is the rate-limiting step in the biosynthesis of catecolamines and has a kcat/Km of 2.64 E7 $M^{-1}s^{-1}$. The expression of TH is activated via a Protein Kinase C (PKC) dependent pathway. Interestingly, the catalytic efficiency of TH is very close to the diffusion limit, justifying the proposal that its activity decreases in microgravity due to an altered rate of diffusion. Furthermore, the membrane translocation of PKC has been shown to be diffusion-limited[11]. It is plausible that this process involving PKC similarly slows down, resulting in a lower level of TH expression. While signal transduction is extremely complex in vivo, PKC has been implicated by several labs with regard to microgravity effects. Specifically, Epidermal Growth Factor (EGF) and 12-*O*-tetradecanoyl-phorbol-13-acetate (TPA) induced expression of c*fos* is inhibited by ~50% in microgravity, whereas forskolin and A23187 induced expression is not altered. EGF, TPA, forskolin and A23187 are all inducers of c*fos* expression; however only EGF and TPA function through a PKC dependent pathway[34].

PKC was also shown to affect lymphocyte locomotion in simulated microgravity. The researchers found that both simulated and real microgravity inhibited locomotion of lymphocytes. They also found that augmentation of the [Ca+2] had no effect, whereas direct activation of PKC via phorbol myristate acetate restores locomotion, further implicating PKC in microgravity effects[35].

NASA engineers developed a Rotating Walled Vessel (RWV), which is basically a cylindrical culture chamber that is rotated at a specific velocity so as to counteract the force of gravity on Earth. The idea is that gene expression in microgravity is also altered by the lack of contact inhibition. In a normal culture environment, the cells sink to the bottom of the culture vessel; the RWV only simulates the turbulent state of cell cultures in microgravity, not true microgravity. Furthermore, it should be noted that additional factors such as shearing forces must be acknowledged during such simulations. Comparisons of gene expression in real microgravity versus simulated microgravity show that the expression of more than 1600 genes changes in real microgravity (see Figure 8). Such a dramatic change indicates that there are many more factors involved that make microgravity effects unique[37]. Regardless, simulated microgravity in a RWV has proven effective in predicting microgravity effects on cellular development. Specifically, the aforementioned induction of cfos via EGF was shown to be inhibited by 30% in a RWV compared to a 50% inhibition in real microgravity[36].

The self-assembly of microtubules is also inhibited by microgravity, presumably due to the macroscopic diffusion process. Microtubule formation is dependent on density gradients, in which they arrange themselves in solution in such a way that the growing (+) end of one microtubule is near the dissociating (-) end of another. The dissociation of the microtubule into free tubulin provides ready material for the (+) end of the second strand, this model is illustrated in Figure 9. Papaseit, et al, proposed that the absence of gravity prevents the formation of density gradients that are necessary for this process to occur.

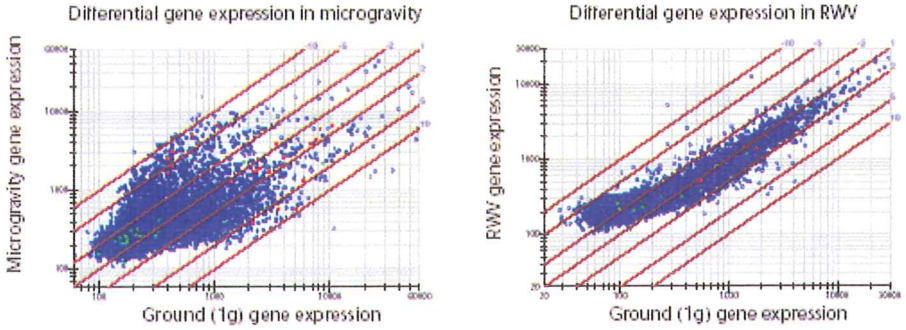

Fig. Gene expression in steady-state cell culture. Human renal cortical cells were cultured for 6d in DMEM/F12, 10% fetal calf serum, on Cytodex-3 beads, then samples were fixed and stored at 7 °C. mRNA was reverse-transcribed with fluorescent bases and analyzed on DNA microarrays (Incyte, Fremont, California). Microgravity (left) and rotating wall vessel (right) were compared with a static non-adherent bag culture grown in parallel; 10,000 genes are represented by individual dots: green dots, shear stress proteins and heat shock proteins; red dots, transcription factors. Genes with similar expression lie on a line from the origin to the top right corner (labeled 1); expression level indicated by distance from the origin. Scale on each axis is $\log_2$.

Figure 8: Deviation from the center diagonal indicates a difference in gene expression. Figure and legend from Hammond et al, 1999.

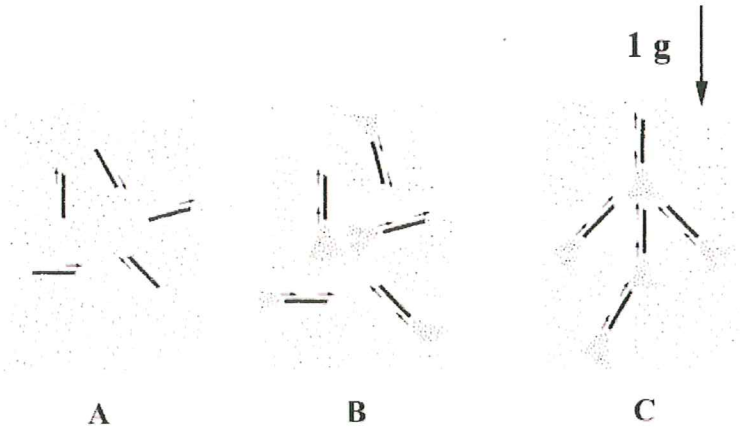

Fig. 5. A possible mechanism for the formation of the self-organized structure. Microtubules are chemically anisotropic, growing and shrinking along the direction of their long axis. This leads to the formation of chemical trails, comprised of regions of high and low local tubulin concentration from their shrinking and growing ends respectively. These concentration trails (density fluctuations) are oriented along the direction of the microtubule. Neighboring microtubules will preferentially grow into regions in which the local concentration of tubulin is highest. When molecular transport is isotropic, microtubules grow and shrink equally in all directions, and the tubulin trails retain an isotropic distribution. For self-organization to occur, this symmetry must be broken. Gravity can do this by introducing a molecular transport term that is faster in the up-down direction. This gives rise to a slight directional bias in the formation of chemical trails. Microtubules will subsequently grow and form preferentially along the direction of these tubulin trails. These processes progressively reinforce themselves, resulting in the development of the periodic changes in microtubule orientation and concentration observed. In *A*, microtubules have just formed from the tubulin solution. They are still in a growing phase and have an isotropic arrangement. In *B*, microtubule disassembly has started to occur at the bifurcation time. This produces trails of high tubulin concentration from the shrinking ends of the microtubules. These macroscopic concentration fluctuations interact with gravity, denser fluctuations drifting downward and lighter ones upwards, leading to an anisotropy in molecular transport. In *C*, microtubules are growing and forming preferentially where the concentration of active tubulin is highest. Anisotropic molecular transport at the bifurcation time privileges microtubule growth along specific directions. Once started, this process subsequently mutually reinforces itself with time and leads to self-organization. When gravity is absent, molecular transport remains isotropic, and self-organization is not triggered.

Figure 9: This figure shows the formation of microtubules in random orientations (A), the concentration gradients that form tubulin dense regions (B) and the higher order organization that results (C). In microgravity the dense clusters of free tubulin at the (-) end fail to form, inhibiting microtubule growth and organization. Figure and legend from Papaseit et al, PNAS, 2000.

With regards to microgravity effects on enzyme kinetics, the Km of lipoxygenases (LOX-1) for free fatty acids has been shown to decrease by a factor of 4, this results in a 4x increase in kcat/Km from 4.4 E^6 $M^{-1}s^{-1}$ to 18.5 E^6 $M^{-1}s^{-1}$. These experiments were performed on the European Space Agency's parabolic flight campaign using their Effect of Microgravity on Enzymatic Catalysis (EMEC) module[39]. Other experiments utilizing the EMEC module have given conflicting evidence that microgravity has no effect on the kinetic parameters of other enzymes, specifically isocitrate lyase[40]. These findings are reconciled in our hypothesis, in which the change in fluid dynamics should affect diffusion-limited processes and have no effect on slower kinetics. It is important to note that the fastest reaction observed for isocitrate lyase (4.4 E^5 $M^{-1}s^{-1}$) is slower than the catalytic efficiency of LOX-1 by an order of magnitude. The acceleration of the kinetics of LOX-1 is interesting because it means that it is possible that gravity, rather than microgravity, could also inhibit some biochemical reactions. Such an inhibition could be explained by considering a protein which requires a very specific orientation with respect to its substrate to bind, the slowing of diffusion would allow for intermolecular forces (e.g. electrostatic steering) to overcome the diffusion of the system. This could hypothetically increase the probability of a binding interaction over a non-binding collision.

Results

In order to examine the kinetics of association between ANS and BSA, the two were rapidly mixed across a range of BSA concentrations and the change in fluorescence was monitored at 470 nm versus time. It is apparent in Figure 10 that the system relaxes to equilibrium faster as the concentration of BSA increases. This faster relaxation is reflected in the time constant, k_{obs}, which was obtained by fitting the raw data from 4 to 5 averaged experiments for each concentration jump to Equations 1 and 2 using the non-linear fit program Origin 5.0 (Figure 11).

The k_{obs} values determined were plotted versus the sum of the equilibrium concentration of BSA and ANS in order to determine the k_{on}, the kinetic rate constant. These plots are shown in Figures 12 and 14, which represent the k_{obs} values obtained from the same raw data sets but fit to different equations to obtain k_{obs} (Equations 1 and 2). Application of linear regression to these plots was used to determine the slope, which is equivalent to the k_{on}. In order to investigate the dependence of the rate constant on viscosity, the experiments were performed in solutions of five different viscosities. As the viscosity of the solution increases with %(v/v) glycerol, the rate of association (k_{on}) of ANS and BSA becomes dramatically slower. Both the standard model (Figure 12 and Equation 1) and the KWW model (Figure 14 and Equation 2) result in a dramatic change in slope as the viscosity increases. The data for both of these plots are summarized in Tables 2 and 4 in the Appendix. The kinematic viscosity of each glycerol solution was determined using a Canon-Fenske viscometer at 6° C. The dynamic viscosities of each solution were determined by multiplying the kinematic viscosity by the density of each solution.

Densities were experimentally determined using a DMA-58 density meter. All density data are also tabulated in the Appendix.

To determine the relationship between the rate of association and viscosity, the values for k_{on} and viscosity were then normalized to relative k_{on} (k_{on}^{o}/k_{on}) and relative viscosity (η/η^{o}) and were plotted. As per the Einstein-Smoluchowski and the Einstein-Stokes relationships (Equations 9 and 10), the rate of a diffusion limited reaction is inversely proportional to the dynamic viscosity of the solution in which it occurs. This predicts a slope of 1.00 for a perfectly diffusion limited reaction when k_{on}^{o}/k_{on} is plotted versus η/η^{o}. The determined slope of 1.62 in Figure 13 is far too large. One possible explanation is that the association of BSA and ANS may have multiple time constants, and thus extremely complex kinetic interactions. In other words, the simple association model $A + B \leftrightarrow C$ may not suffice.

In order to determine if another model could compensate for possible complex molecular mechanisms, the k_{obs} values were also determined by fitting the relaxation curves to the KWW model (Equation 2), using $\beta = .6$ as a constant. The sum of the concentration was also multiplied by the stoichiometric ratio of [BSA]/[ANS] in order to more accurately estimate equilibrium concentrations (see page 16). As shown in Figure 12, k_{on} was determined for each glycerol concentration by determining the slope of the lines in this plot.

These values for k_{on} were also normalized and plotted versus normalized viscosity (Figure 15). When the data are fit using k_{obs} values from the KWW, a realistic slope (1.05) for a diffusion limited reaction is obtained; however, the values of the individual rates are now far slower than

the expected range for a diffusion controlled reaction. The large number of potential binding sites on BSA for ANS was the primary motivation to use the KWW model, which is normally used to fit complex relaxation data with multiple (>5) time constants (τ or k_{obs}) that appear to occur as single molecular event.

In order to estimate the purity of the protein samples, Fatty Acid Free BSA (FAF-BSA) and Fraction V BSA (both purchased from Sigma) were thermally denature in a Microcal Differential Scanning Calorimeter. These curves are shown in Figure 16. The apparent reduction of the noise in the calorimetric denaturation of FAF_BSA relative to Fraction V and the shift in Tm are indicative of a higher purity; however, the remaining noise in the FAF-BSA curve is far from ideal. These data were used to select FAF-BSA as the BSA subtype used in the experiments described. A direct steady-state titration of ANS into BSA was performed on a Fluormax fluorometer using a 1 cm quartz cuvette in order to determine the Kd (36 nM). The titration and best fit to a single site isotherm are shown in Figure 17.

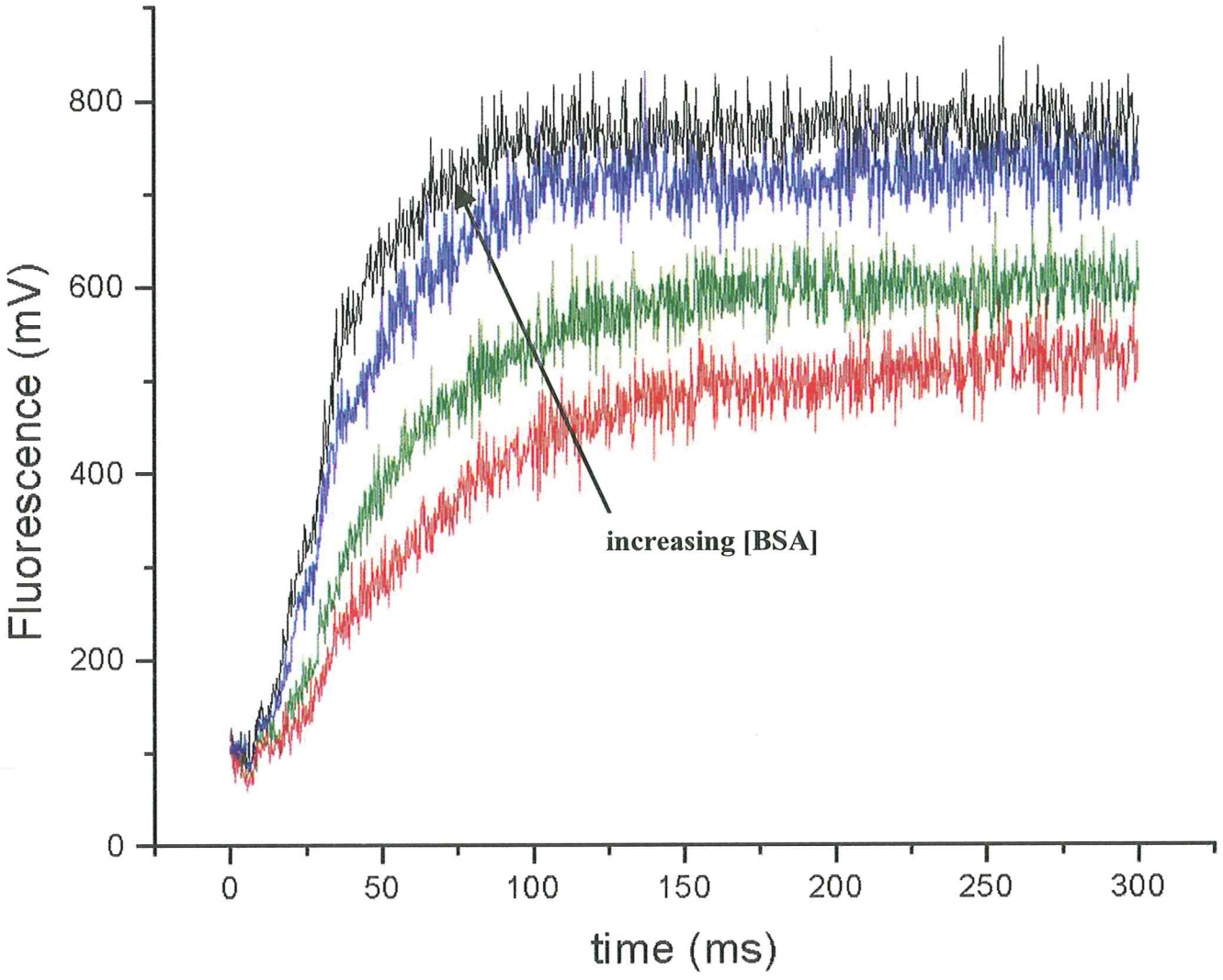

Figure 10: Raw relaxation data demonstrating the change in the time constant (k_{obs}) as the [BSA] increases with each concentration jump.

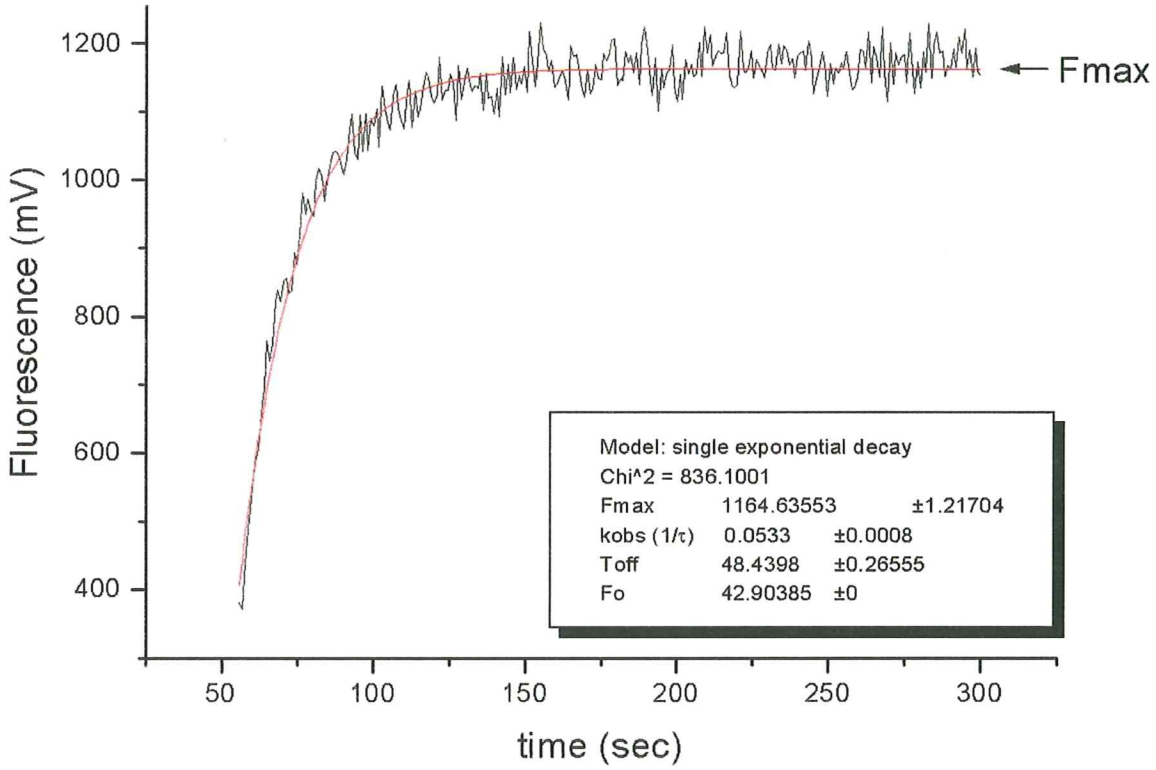

Figure 11: Fit relaxation data using the non-linear fit program Origin 5.0. 1.1 uM BSA + 1.0 uM ANS. Excitation @ 280 nm, Emission at 468 nm.

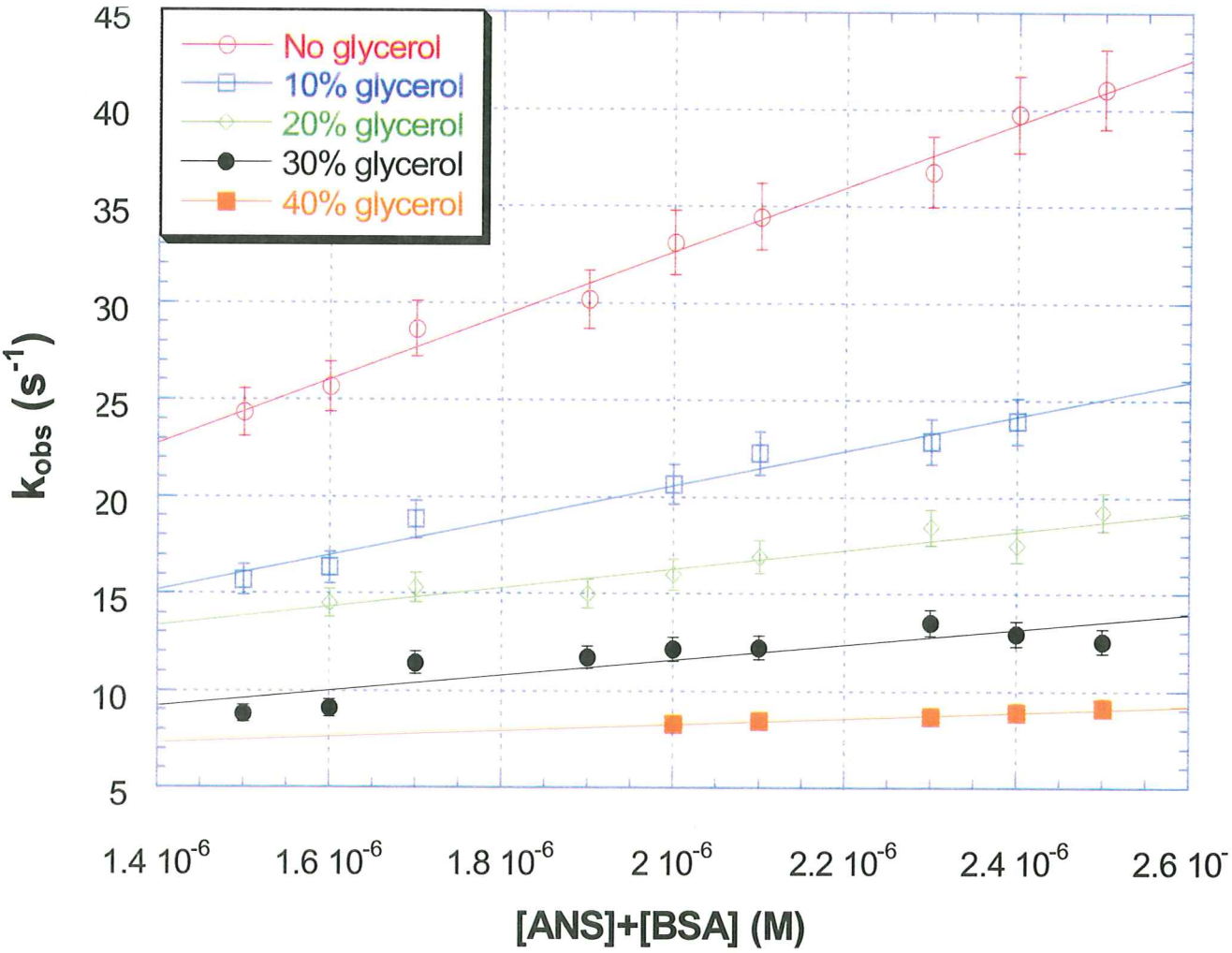

Figure 12: Viscosity dependence of the association of BSA and ANS using k_{obs} values from the standard A + B ↔ C relaxation model. The slope of each line is the k_{on}.

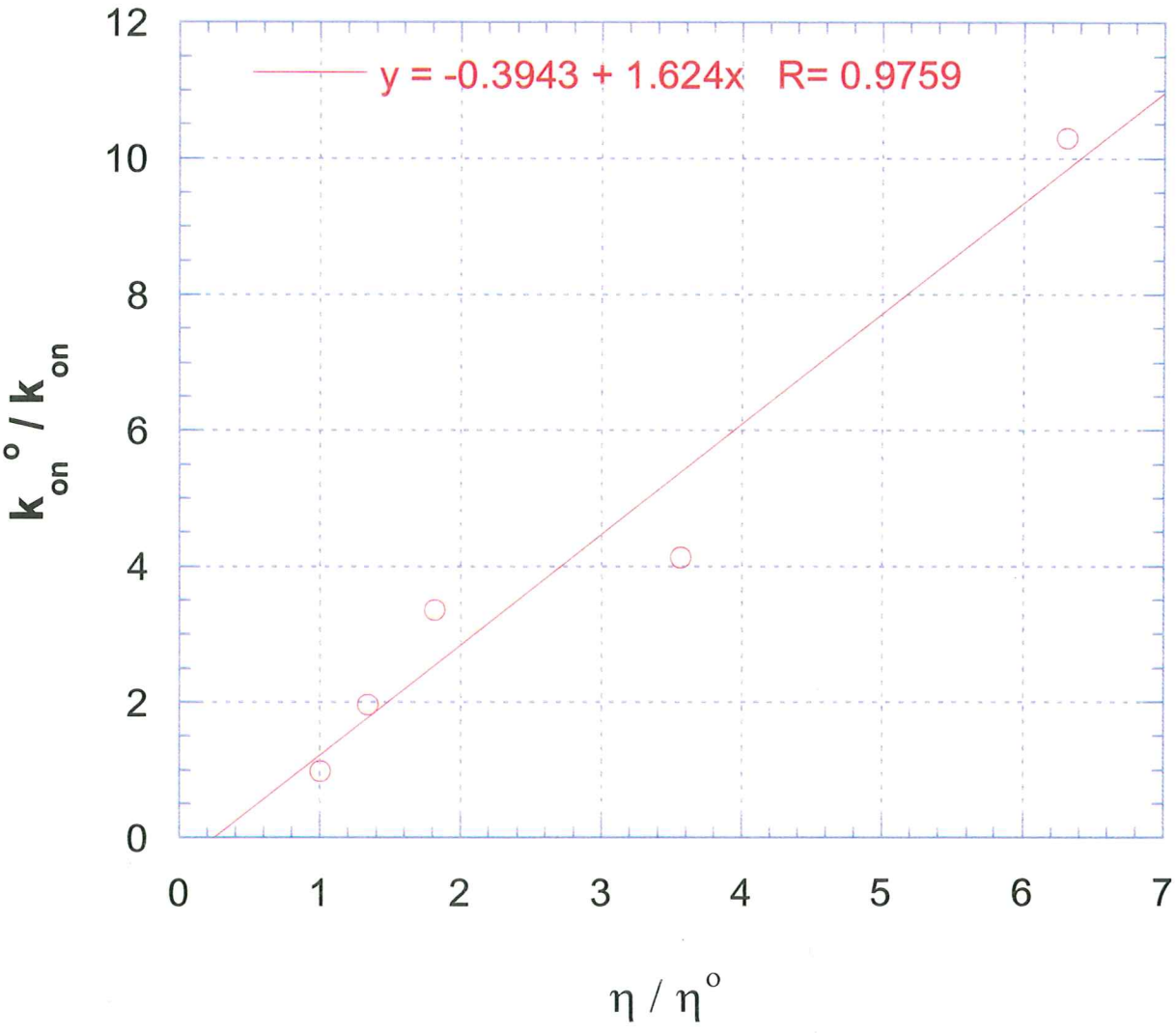

Figure 13: Relative viscosity dependence on the relative k_{on} for a simple A + B ↔ C relaxation model. Values for k_{on} were determined from the slopes in Figure 12.

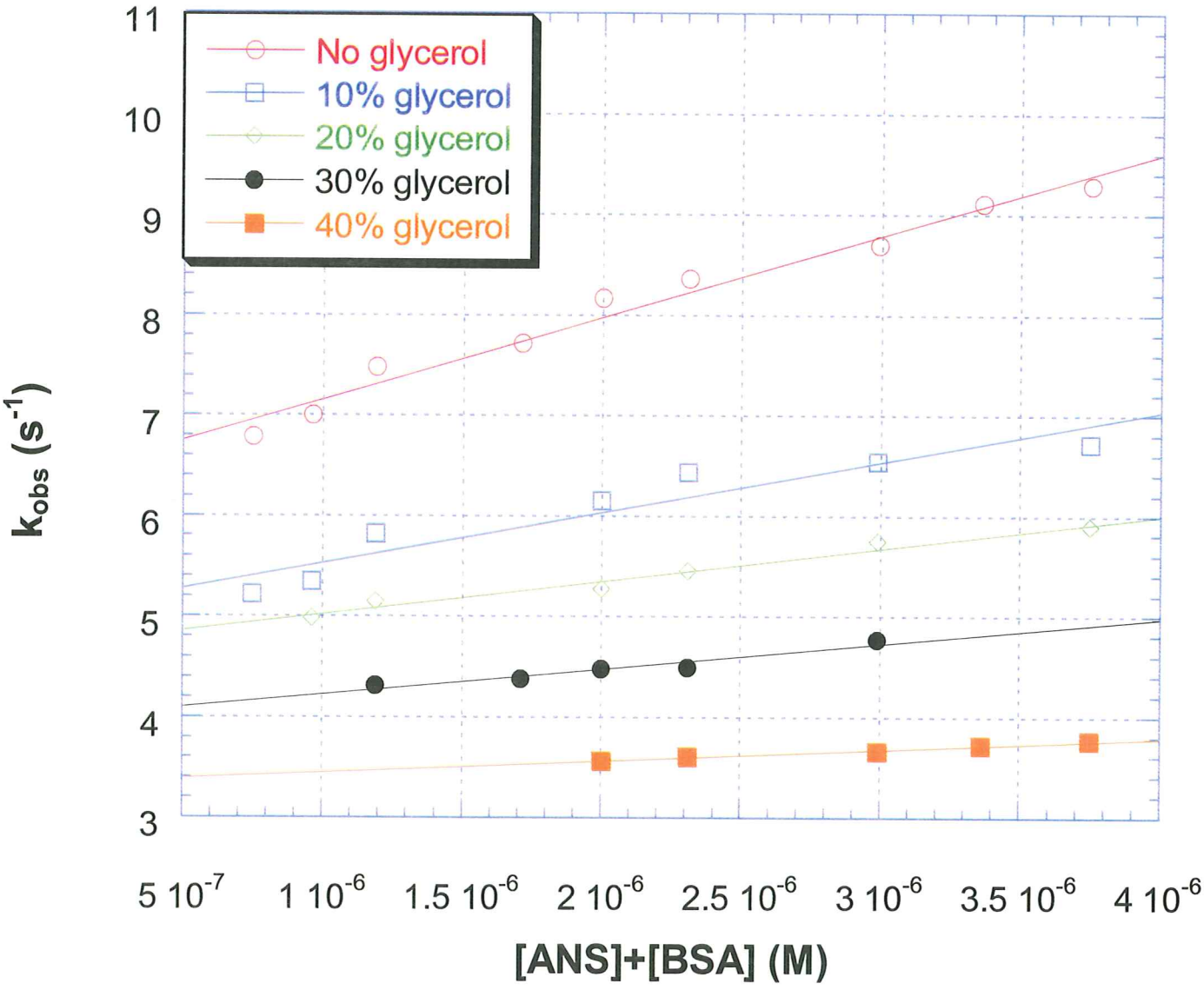

Figure 14: Viscosity dependence of the association of BSA and ANS using k_{obs} values from the KWW model, where $\beta = .6$

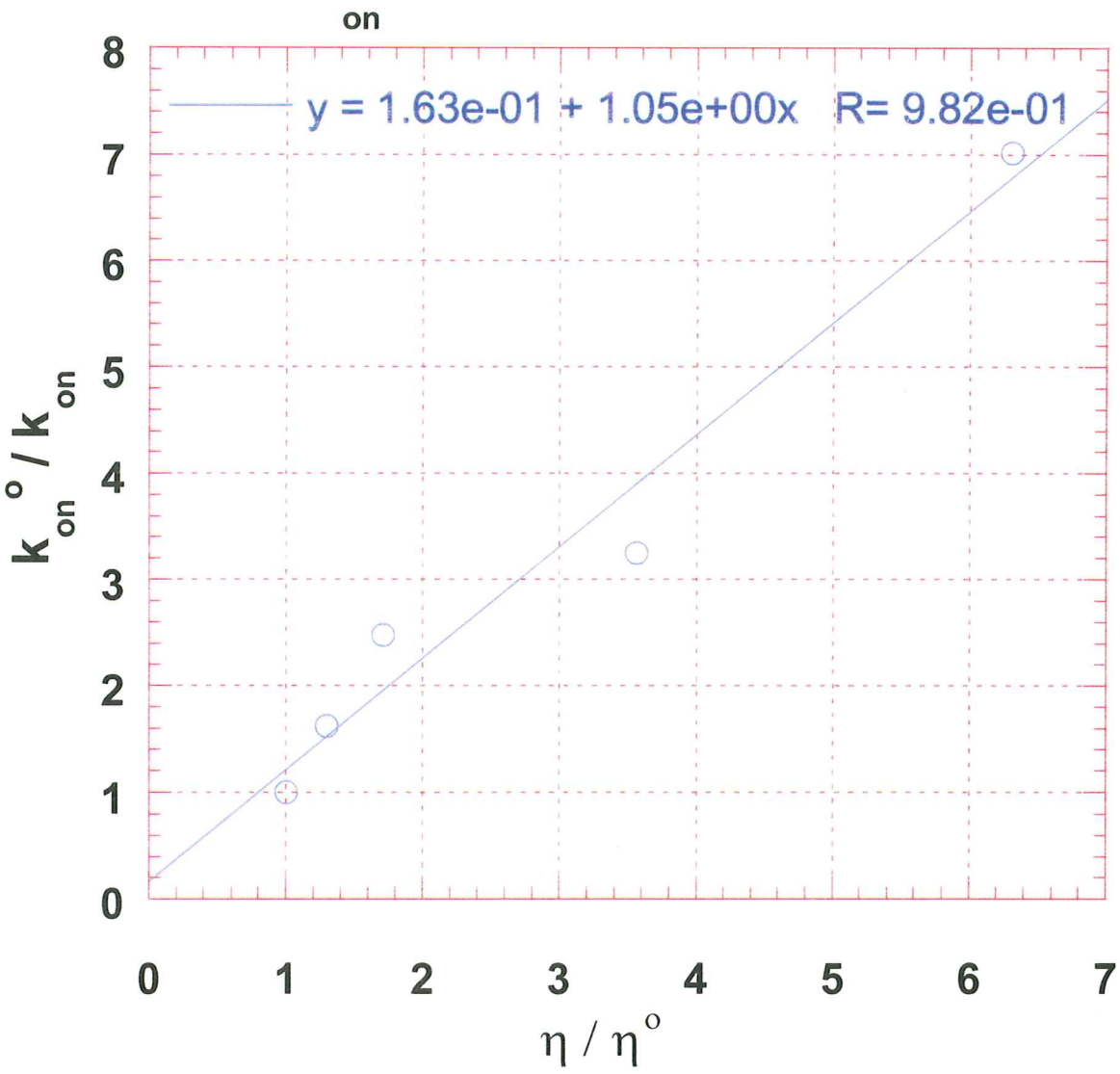

Figure 15: Relative viscosity dependence of the relative k_{on} for BSA + ANS using the k_{on} values determined the KWW model (Figure 14).

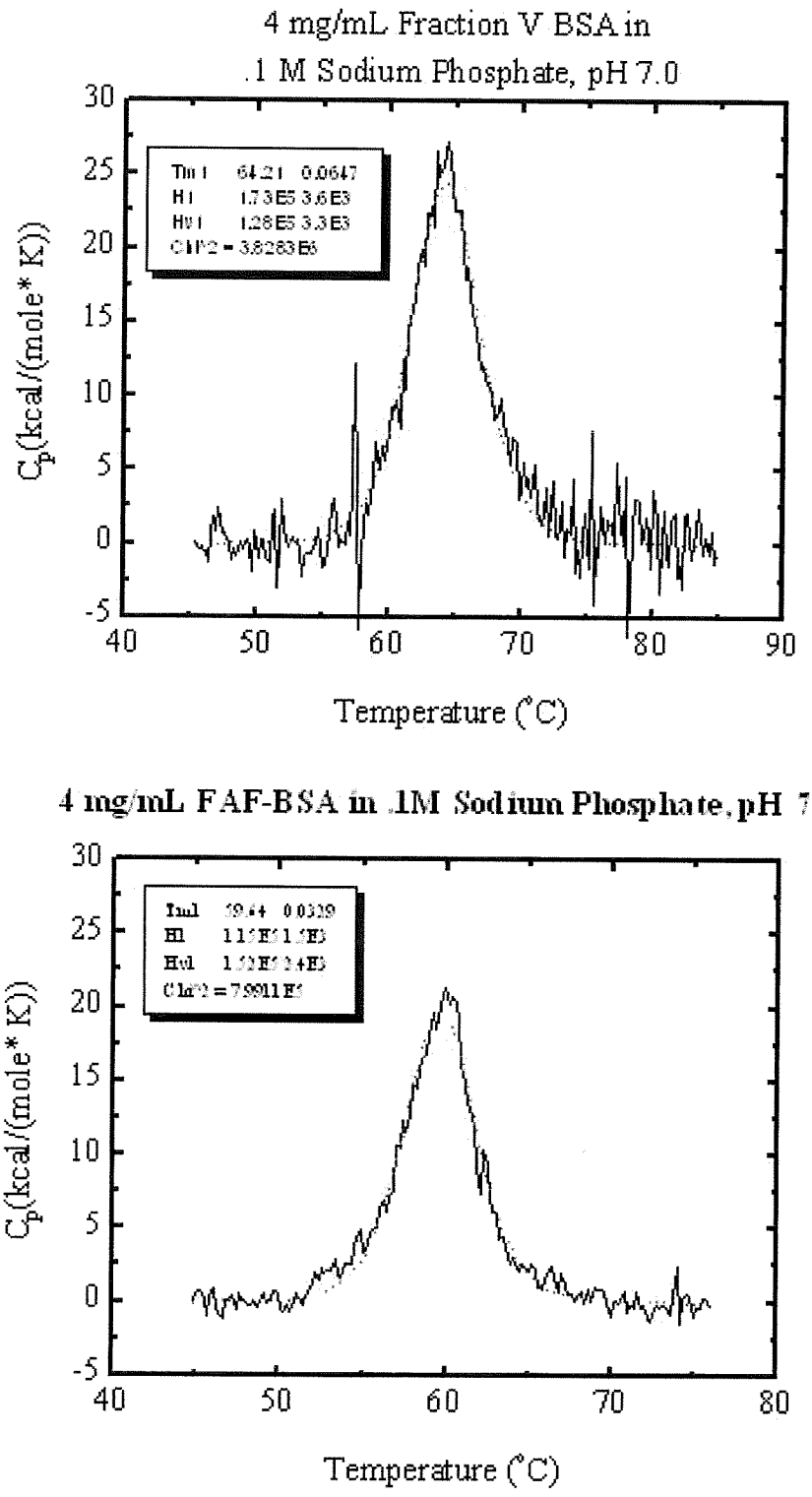

Figure 16: Differential Scanning Calorimetric traces for the denaturation of two different BSA subtypes purchased from Sigma. Top panel shows Fraction V BSA; bottom panel shows Fatty-Acid Free BSA. Note that the Tm for Fraction V is ~ 5° C higher than FAF-BSA.

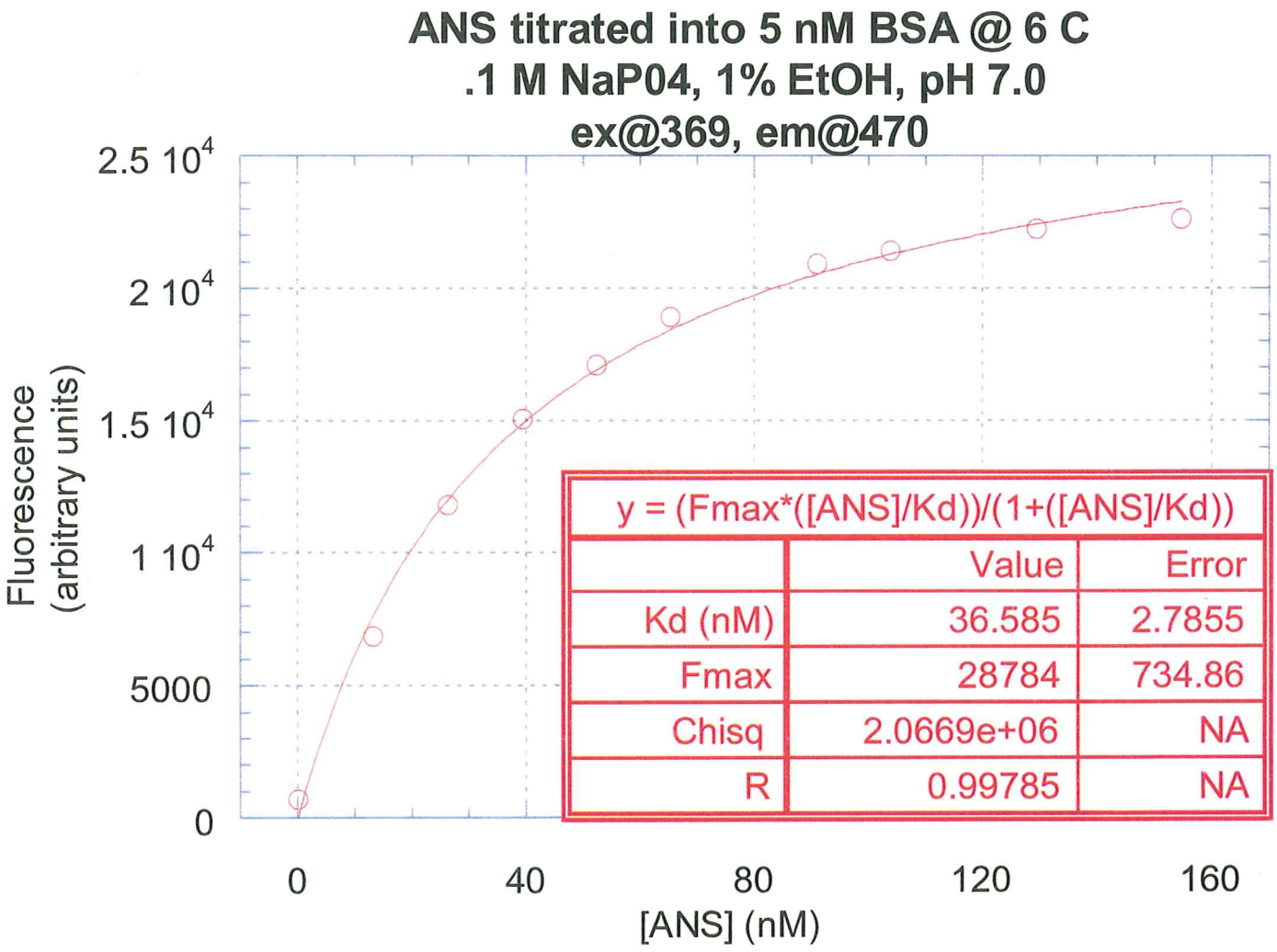

Figure 17: A direct binding assay was performed at steady-state in order to determine the Kd for the binding of ANS to BSA, which appears to be non-cooperative.

Discussion

Despite fitting the collected data to several different models to determine if the association of BSA and ANS is diffusion-limited, the results of the experiments described in this thesis are still inconclusive. The k_{on} values determined by the fits to the standard A+B↔C single exponential model are consistent with the a diffusion-limited reaction; however, the effect of the relative viscosity of the solution does not appear to be perfectly inverse to the relative rate (k_{on}). Likewise, when the data is fit the KWW model and β is set to .6, the relationship becomes perfectly inverse (i.e. a slope of 1 is obtained in Figure 15); however, the values for k_{on} disagree with the rates predicted for a diffusion-limited reaction as per the Einstein-Smoluchowski model.

It is unclear whether these disagreements with the predicted behavior for the BSA-ANS system arise from complex kinetic interaction between the protein and ligand or from interaction of the protein with the glycerol, which is a previously noted problem with the methods employed for this thesis. In order to determine whether glycerol is directly affecting the kinetics, another viscogenic agent such as sucrose should be used.

An alternative explanation for the data obtained is that the association of BSA and ANS is simply too kinetically complicated to be observed either with the techniques used thus far. Figure 4 shows all the possible binding sites for ANS on a molecule of HSA, which we can consider homologous to BSA. There are over 100 binding site; however, only the sites in hydrophobic pockets cause ANS to fluoresce upon binding. The approximate 1:1 stoichiometric ratio for mixing was initially chosen under the assumption that a single binding site on BSA may bind tighter than the other possible sites. This may not be true, which is why the data was fit to

the KWW model (Equation 2). The stretched relaxation should correct for discrepancies in the data that arise from multiple time constants; however, this method has not been utilized for this particular purpose before and it is unclear whether the results are real or simply a chance correlation. The simple disagreement between the predicted values of k_{on} and the experimentally determined values using this model make the results inconclusive. Furthermore, if multiple sites with significantly altered on-rates were present on BSA, then the equilibrium titrations shown in Figure 17 should reflect this as well.

On definitive conclusion from these experiments is that the association of BSA and ANS is clearly and dramatically slowed by increasing viscosity. This is a hallmark of diffusion controlled reactions. Even though we have not yet established the correct molecular/kinetic mechanism to quantitatively account for the viscogenic effects on the reactions, we have established that altering the rate of diffusion in solution alters the rate of this reaction, making it at least a qualitative indicator reaction of the detection of diffusion mediated effects of microgravity.

Literature Cited

1. DeLucas LJ, Smith CD, Carter DC, Twigg P, He XM, Snyder RS, Weber PC, Schloss JV, Einsahr HM, Clancy LL, McPherson A, Koszelak S, Vandonselaar MM, Prasad L, Quail JW, Delbaere LT and Buff CE (1992) *Adv. Space Res.* 12:393-400

2. Berg JM, Tymoczko JL and Stryer L (2001) *Biochemistry*, 5th ed. W.H. Freedman and Company, New York.

3. Bazelyansky M, Robey E and Kirsch JF (1986) *Biochemistry* 25: 125-130.

4. Kurz LC, Weitkamp E and Frieden C (1986) *Biochemistry* 26: 3027-3032.

5. Hardy LW and Kirsch JF (1984) *Biochemistry* 23: 1275-1282.

6. Pocker Y and Janjie N (1987) *Biochemistry* 26: 2597-2606.

7. Brouwer AC and Kirsch JF (1982) *Biochemistry* 21: 1502-1507.

8. McKinnie RE and Olson JS (1981) *J. Biol. Chem.* 256: 8928-8932.

9. Koren R and Hammes GG (1976) *Biochemistry* 15: 1165-1171.

10. Patrick SM and Turchi JJ (2001) *J. Biol. Chem.* 276: 22630-22637.

11. Schaefer M, Albrecht N, Hofmann T, Gudermann T and Schultz G (2001) *FASEB* 15:1634-1636.

12. Kholodenko BN, Brown GC and Hoek JB (2000) *Biochem. J.* 350: 901-907.

13. Blacklow SC, Raines RT, Lim WA, Zamore PD and Knowles JR (1988) *Biochemistry* 27: 1158-1167.

14. Fekkes P, den Blaauwen T and Driessen AJM (1995) *Biochemistry* 34: 10078-10085.

15. Chrunyk BA and Matthews R (1990) *Biochemistry* 29: 2149-2154.

16. Muderhwa JM and Brockman HL (1992) *J. Biol. Chem.* 267: 24184-24192.

17. Kelemen BR and Raines RT (1999) *Biochemistry* 38: 5302-5307.

18. Agutter PS, Malone PC and Wheatley DN (2000) *J. Hist. Biol.* 33: 71-111.

19. Nakatani H, Haga M and Hiromi K (1974) *FEBS Letters* 43: 293-296.

20. Regenfuss P and Clegg RM (1987) *Biophys. Chem.* 26: 83-89.

21. Sambrook J and Russell (2001) *Molecular Cloning: A Laboratory Manual* Cold Spring Harbor Laboratory Press, Cold Spring Harbor.

22. Fitos I, Visy J and Kardos J (2002) *Chirality* 14: 442-448.

23. Chang L, Wen E, Hung J and Chang C (1994) *J. Protein Chem.* 13: 635-640.

24. Matulis D and Lovrien R (1998) *Biophys. J.* 74, 422-429.

25. Sugio S, Kashima A, Mochizuki S, Noda M and Kobayshi K (1999) *Portein Eng.* 12:439.

26. Bernasconi CF (1976) *Relaxation Kinetics* Academic Press, New York.

27. Siegal J, Benny Lee KC, Webb SED, Leveque-Fort S, Cole MJ, Jones R, Dowling D, French PMW and Leer MJ (2001) *Biophys. J.* 81:1265-74.

28. Metzler R, Klafter J and Jortner J (1999) *Proc. Natl. Acad. Sci. USA* 96, 11085-11089.

29. Caldin EF (1964) *Fast Reactions in Solution* John Wiley & Sons Inc, New York.

30. Espenson JH (1995) *Chemical Kinetics and Reaction Mechanisms* 2nd ed. McGraw-Hill Inc, New York.

31. van Holde KE (2002) *Biophys. Chem.* 101-102: 249-254.

32. Stroppolo ME, Falconi M, Caccuri AM and Desideri A (2001) *Cell. Mol. Life Sci.* 58: 1451-1460.

33. Lelkes PI, Ramos RM, Chick DM, Liu J and Unsworth BR (1994) *FASEB* 8: 1177- 1182.

34. De Groot RP, Rijken PJ, Den Hertog J, Boonstra J, Verkleij AJ, De Laat SW and Kruijer W (1991) *Exp. Cell Res.* 197: 87-90.

35. Sundaresan A, Risin D and Pellis NR (2002) *In Vitro Cell. Dev. Biol. – Animal* 38:118-122.

36. De Groot RP, Rijken PJ, Den Hertog J, Boonstra J, Verkleij AJ, De Laat SW and Kruijer W (1990) *J. Cell Sci.* 97: 33-38.

37. Hammond TG, Lewis FC, Goodwin TJ, Linnehan RM, Wolf DA, Hire KP, Campbell WC, Benes E, O'Reilly KC, Globus RK and Kaysen JH (1999) *Nature Med.* 5: 359.

38. Papaseit C, Pochon N and Tabony J (2000) *Proc. Natl. Acad. Sci. USA* 97: 8364-8368.

39. Maccarrone M and Finazzi-Agro A (2001) *FEBS Letters* 489: 283.

40. Ranaldi F, Vanni P and Giachetti E (2003) *Biophys. Chem.* 103: 169-177.

41. Schoeffler AJ, Ruiz CR, Joubert AM, Yang X and LiCata VJ (2003) *J. Biol.Chem.* 278:33268-75.

Appendix

Table 1: The kinematic viscosity and density of each solution was measured directly in order to calculate dynamic viscosity.

% glycerol	Kinematic viscosity (centistokes)	Density (g/cm^3)	Dynamic viscosty (Pascal•seconds)
0	1.5827	1.012005	1.60E-03
10	2.0504	1.04401	2.14E-03
20	2.6990	1.073185	2.90E-03
30	5.1795	1.101015	5.70E-03
40	8.9174	1.13255	1.01E-02

Table 2: Time constants determined for the concentration of [ANS+BSA] at each concentration jump when fit to a standard A+B→C relaxation model.

[ANS]+[BSA] (M)	kobs (s^{-1}) No glycerol	kobs (s^{-1}) 10% glycerol	kobs (s^{-1}) 20% glycerol	kobs (s^{-1}) 30% glycerol	kobs (s^{-1}) 40% glycerol
1.50E-06	24.36	15.71	—	8.84	—
1.60E-06	25.68	16.33	14.51	9.11	—
1.70E-06	28.66	18.82	15.31	11.43	—
1.90E-06	30.19	—	14.99	11.73	—
2.00E-06	33.14	20.65	15.99	12.16	8.32
2.10E-06	34.48	22.27	16.895	12.23	8.51
2.30E-06	36.79	22.88	18.43	13.52	8.73
2.40E-06	39.77	—	17.5	—	8.95
2.50E-06	41.08	23.92	19.23	—	9.16

Table 3: Relative k_{on} and η for the association of BSA and ANS when fit to a standard A+B→C relaxation model.

% glycerol	Dynamic viscosity (Pascal*seconds)	kon ($M^{-1}s^{-1}$)	η/η^{o}	k_{on}^{o} / k_{on}
0	1.60E-03	1.65E+07	1.00	1.00
10	2.14E-03	8.41E+06	0.51	0.75
20	2.90E-03	4.92E+06	0.30	0.55
30	5.70E-03	3.99E+06	0.24	0.28
40	1.01E-02	1.60E+06	0.10	0.16

Table 4: Time constants determined for the equilibrium concentration of [ANS+BSA] at each concentration jump when fit to the KWW stretched relaxation model. $\beta = .6$

[ANS]+[BSA] (M)	kobs (s^{-1}) No glycerol	kobs (s^{-1}) 10% glycerol	kobs (s^{-1}) 20% glycerol	kobs (s^{-1}) 30% glycerol	kobs (s^{-1}) 40% glycerol
7.50E-07	6.79	5.22	—	—	—
9.60E-07	7.01	5.34	4.98	—	—
1.19E-06	7.49	5.82	5.14	4.31	—
1.71E-06	7.73	—	—	4.38	—
2.00E-06	8.17	6.15	5.28	4.48	3.57
2.31E-06	8.37	6.44	5.45	4.49	3.61
2.99E-06	8.70	6.54	5.75	4.77	3.67
3.36E-06	9.11	—	—	—	3.72
3.75E-06	9.29	6.72	5.89	—	3.78

Table 5: Relative k_{on} and η for the association of BSA and ANS when fit to the KWW stretched relaxation model. $\beta = .6$

% glycerol	Dynamic viscosty (Pascal*seconds)	kon ($M^{-1}s^{-1}$)	η/η^{o}	k_{on}^{o} / k_{on}
0	1.60E-03	8.15E+05	1.00	1.00
10	2.14E-03	5.02E+05	1.30	1.62
20	2.90E-03	3.29E+05	1.71	2.48
30	5.70E-03	2.51E+05	3.56	3.25
40	1.01E-02	1.16E+05	6.31	7.02

Acknowledgements

First, I would like to thank my thesis advisor and mentor, Vince LiCata, for the infinite patience, guidance and inspiration he has granted me over the past four years. I came into his lab seeking experience, but I have left with so much more; for that I will always be grateful. His passion for learning and science is absolutely contagious.

I also want to thank everyone in the LiCata lab: Carmen Ruiz for her mother-like badgering and laboratory lessons, Dr. Kausiki Datta for all her technical advice and her warm smile, Dr. Chin-Chi (Kitty) Liu for her beautiful personality, infinite patience and endless problem solving skills, Allison Joubert for her late night trouble shooting discussions, Greg Thompson for all his help with the Stopped-Flow, Daniel Deredge for his discussions and debates about corporate politics in science, and Allyn Schoeffler for introducing me to my first biochemical experiment.

I am also indebted to the members of my class who have pulled me through late nights of cramming and helped me to solve seemingly unsolvable problems. They include: Beth Reimer, Jenna Traylor Ortego, Andy Wowor, Thomas Medler and Ben Trappey. I must also thank my roommate, James Fountain, for his patience and tolerance of the study habits of myself and my friends.

Special thanks go to my committee members, Dr. James Moroney and Dr. Britt Thomas, whom I am grateful for their willingness to serve on my committee.

I am infinitely grateful for the love, patience and grace that Claire Dawkins has brought into my life. I thank her for all the late night walks and conversations that led to my decision to pursue research over medicine. Her endless support is absolutely unparalleled.

I must also thank Dr. Robert McMahon for his intellectual stimulation. He has been a truly amazing teacher and mentor over the past two years and his challenges and lessons will forever bear on my mind and soul.

Finally I want to thank all of my friends and family who have morally, spiritually and financially supported me throughout the years in my pursuit of learning.